Structure of Nanocrystalline Materials with Intrinsic Disorder from Atomic Pair Distribution Function Analysis: The Intercalation Compound Ag_xMoS_2

Seong-Ju Hwang,[†] Valeri Petkov,[‡,§] K. Kasthuri Rangan,[†] Sarvjit Shastri,[||] and Mercouri G. Kanatzidis[†,*]

Department of Chemistry and Center for Fundamental Materials Research, Michigan State University, East Lansing, Michigan 48824, Department of Physics and Astronomy and Center for Fundamental Materials Research, Michigan State University, East Lansing, Michigan 48824, and Advanced Photon Source, Argonne National Laboratory, Argonne, Illinois 60439

Received: June 20, 2002

The full three-dimensional structure of Ag-intercalated molybdenum disulfide has been experimentally determined. The atomic pair distribution function (PDF) analysis technique has been employed because of the very limited structural coherence in this nanocrystalline material. We found that at the atomic scale, this compound can be well-described as an assembly of anionic MoS_2 slabs encapsulating the Ag^+ ions. Silver is found in an almost linear coordination of two sulfur atoms at 2.41 and 2.46 Å. The molybdenum atoms engage in strong metal−metal bonding giving rise to Mo−Mo zigzag chains within the MoS_2 slabs. This study demonstrates the effectiveness of PDF technique in determining the structure of poorly diffracting, heavily disordered, and nanocrystalline materials. The new structural information obtained for Ag_xMoS_2 could not have been obtained by any other currently available technique.

Introduction

The exfoliation of MoS_2 into nanosheets using its lithiated form, $LiMoS_2$[1], marked a turning point in the utility of this material as an intercalation host for a large variety of species.[1−3] The intercalation into MoS_2 is thus a multistage process: first, lithium is inserted in pristine 2H−MoS_2 and the resulting $LiMoS_2$ is exfoliated into a colloidal suspension by reacting with water. Then, appropriate chemical species are added into the suspension, and finally, the MoS_2 layers are restacked with the chemical species included. This "soft chemistry" (chimie douce[4]) process can be called "encapsulative restacking", and several hybrid systems such as polymer−MoS_2,[2,5] $Al_{13}O_4(OH)_{24}(H_2O)_{12}$−$MoS_2$,[6] $Co_6Q_8(PR_3)_6$−MoS_2 (Q = S, Se, and Te, and R = alkyl),[7] Ag_xMoS_2,[8] and Hg_xMoS_2[9] have been prepared through this route. Alternatively, in the absence of a "guest" species, the restacking process results in so-called *r*-MoS_2, which has been shown to be a slightly reduced material (e.g., $LiMoS_2$ or H_xMoS_2 depending on pH with $x < 0.1$).[10] In all cases, the products have low dimensional layered structures, poor crystallinity, and disorder that make it difficult to solve their structure through traditional crystallographic techniques including Rietveld refinement. Local probe techniques such as extended X-ray absorption fine structure (EXAFS) can provide useful local structure information but do not allow a complete three-dimensional (3D) structure determination.[8,9,11] The structures of $LiMoS_2$ and restacked WS_2 were recently determined with the atomic pair distribution function (PDF) technique.[12,13] Restacked WS_2 was found to possess zigzag W−W chains with very short, < 2.8 Å, W−W bonds.[13] On the other hand, $LiMoS_2$ (precursor to exfoliation) was found to exhibit an interesting clustering of Mo atoms into chains of Mo_4−diamond-shaped tetramers.[12b] The PDF technique proved successful because it utilized all components of the diffraction data including Bragg as well as diffuse scattering and thus reflected both the average atomic structure and the local deviations from it. This is in contrast to the traditional crystallographic techniques, which rely on sharp Bragg peaks alone,[14] and thus give information only about the average structure.

Recently, a Ag-intercalated MoS_2 ($Ag-MoS_2$) phase was prepared and studied by EXAFS.[8a] The study concluded that the Ag atoms are coordinated by two S atoms at 2.43 Å. Also, it suggested that MoS_2 layers are very likely to be a mixture of the so-called 1T−MoS_2 and 2H−MoS_2 phases. However, the full 3D structure has not been determined and remains an outstanding issue because $Ag-MoS_2$ is too disordered and poorly diffracting to lend itself to the traditional techniques of structure determination. In the present study, we employ the PDF technique to determine the structure of $Ag-MoS_2$. We find that the structural coherence of $Ag-MoS_2$ is limited only to ∼25 Å, and in this sense, the material is deemed nanocrystalline. Nevertheless, it has a well-defined 3D atomic ordering featuring zigzag chains of distorted MoS_6 octahedra and pseudolinear AgS_2 units. No impurity 2H−MoS_2 phase was found. This atomic arrangement can be fully described by a monoclinic unit cell with four formula units of $Ag_{0.4}MoS_2$. Knowledge of the structure at the level of detail achieved in this work is important to facilitate a better understanding and even utilization of the material's properties.

Experimental Section

Sample Preparation. The sample was prepared through an exfoliation/restacking route that is similar but not identical to the method used in the previous EXAFS study.[8a] First, $LiMoS_2$ was prepared by reacting pristine MoS_2 with excess $LiBH_4$[15] that was then exfoliated by soaking in deionized water. The colloidal MoS_2 was thoroughly washed with water to remove LiOH. Ag^+ ions were inserted between the MoS_2 slabs by adding $AgNO_3$ into the solution. The product was isolated by

* To whom all the correspondence should be addressed. E-mail: kanatzid@cem.msu.edu.

[†] Department of Chemistry and Center for Fundamental Materials Research, Michigan State University.

[‡] Department of Physics and Astronomy and Center for Fundamental Materials Research, Michigan State University.

[§] Present address: Department of Physics, Central Michigan University, Mt. Pleasant, MI 48859.

[||] Argonne National Laboratory.

10.1021/jp0263469 CCC: $22.00
Published on Web 11/07/2002

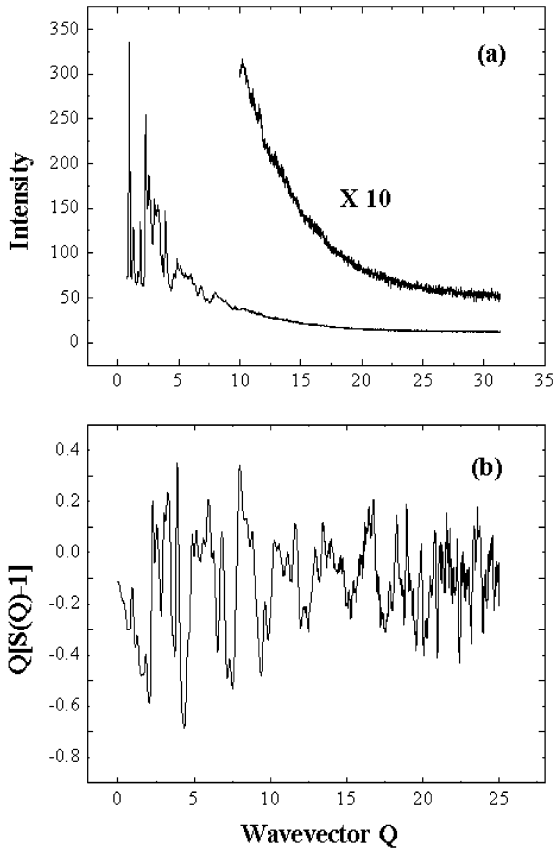

Figure 1. Powder diffraction pattern (a) and reduced $Q[S(Q) - 1]$ structure factor (b) for $Ag_{0.4}MoS_2$ ($\lambda = 0.1534$ Å). The inset in panel (a) represents the high-Q region of the data in an expanded scale.

filtration, washed with water, and finally dried under vacuum. The stoichiometry of the material was determined by microprobe energy dispersive spectroscopic (EDS) analysis and found to be $Ag_{0.4}MoS_2$.

X-ray Diffraction (XRD) Experiments. The XRD measurements were carried out at the SRI-CAT 1-ID beam line at the Advanced Photon Source, Argonne. The sample was carefully packed between Kapton foils to avoid texture formation and subjected to measurements with X-rays of energy 80.725 keV ($\lambda = 0.1534$ Å). The higher energy X-rays were used to extend the region of observable reciprocal space (i.e., to obtain data at higher wave vectors Q), which is important for the success of PDF analysis. Scattered radiation was collected with an intrinsic germanium detector coupled to a multichannel analyzer. Several runs were conducted, and the resulting XRD patterns were averaged to improve the statistical accuracy and to reduce any systematic effect due to instabilities in the experimental setup. The XRD pattern obtained was plotted in Figure 1a as a function of the wave vector Q. Only a few Bragg-like peaks were observed at low values of Q. These peaks were considerably broadened and already merged into a slowly oscillating diffuse component at approximately ~8 Å^{-1}. Such a pattern, which is usually observed with significantly disordered materials, is practically impossible to be tackled by traditional tools for structure determination such as the Rietveld technique. However, as we demonstrate later, once reduced to the corresponding atomic PDF, experimental diffraction data becomes a structure sensitive quantity, lending itself to structure determination.

PDF Analysis of the Diffraction Data. The frequently used atomic PDF, $G(r)$, is defined as follows:

$$G(r) = 4\pi r[\rho(r) - \rho_o] \qquad (1)$$

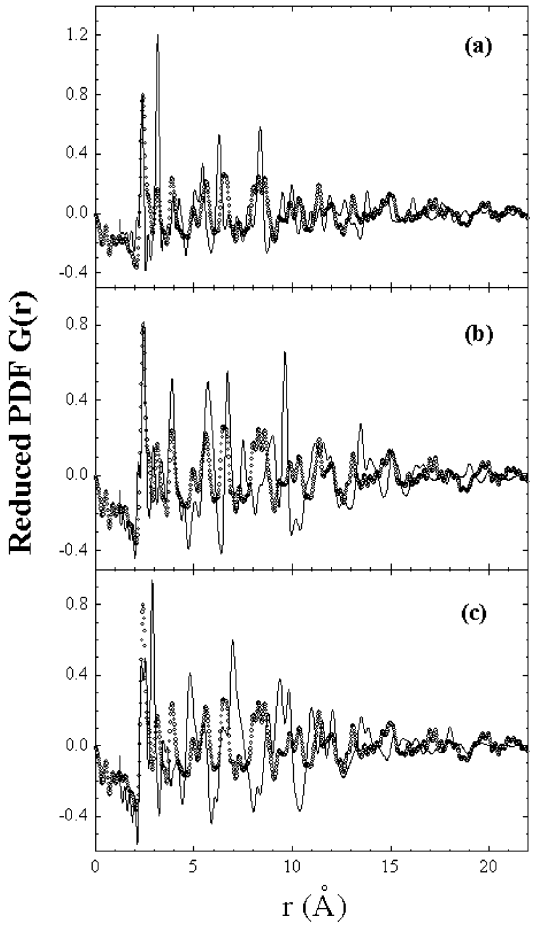

Figure 2. Comparison between the experimental PDF for $Ag_{0.4}MoS_2$ (circles) and model PDFs (line) based on (a) hexagonal 2H−MoS_2 type structure, (b) triclinic $LiMoS_2$ type structure predicted by ab initio simulations,[19] and (c) triclinic $LiMoS_2$ type structure obtained from a PDF study.[9b] The model (a) has a linear AgS_2 moiety while the silver ions in models (b) and (c) are located in the Li site in the previously reported triclinic lattices (refs 12b and 24).

where $\rho(r)$ and ρ_o are the local and average atomic number densities, respectively, and r is the radial distance. $G(r)$ gives the number of atoms in a spherical shell of unit thickness at a distance r from a reference atom. It peaks at characteristic distances separating pairs of atoms and hence reflects the atomic structure. $G(r)$ is the Fourier transform of the experimentally observable total structure factor,[16] $S(Q)$, i.e.,

$$G(r) = (2/\pi) \int_{Q=o}^{Q_{max}} Q[S(Q) - 1] \sin(Qr)\, dQ \qquad (2)$$

where Q is the magnitude of the wave vector ($Q = 4\pi \cdot \sin\theta/\lambda$). The structure factor (essentially normalized intensity $S(Q)$) is related to the coherent part of the total diffracted intensity of the material as follows:

$$S(Q) = 1 + [I^{coh}(Q) - \sum c_i |f_i(Q)|^2]/|\sum c_i f_i(Q)|^2 \qquad (3)$$

where $I^{coh}(Q)$ is the coherent scattering intensity per atom in electron units and c_i and f_i are the atomic concentration and X-ray scattering factor, respectively, for the atomic species of type i. The reduced structure factor $Q[S(Q) - 1]$ extracted from the powder XRD pattern of Figure 1a is shown in Figure 1b. The corresponding atomic PDF, $G(r)$, is plotted in Figure 2. All data processing was done using the program RAD.[17] A comparison between the data in Figure 1a,b exemplifies the substantially different way the same diffraction features show

up in the powder XRD patterns and in the corresponding structure factors after intensity normalization according to eq 3. The XRD pattern in Figure 1a is dominated by strong Bragg-like peaks at lower Q values, and in this form, it is mainly sensitive to long-range atomic ordering in materials. However, normalized scattering structure factors extracted from the XRD pattern according eq 3, all of the diffraction features including those at higher values of Q appear equally strong (see Figure 1b). This enhances the sensitivity to local atomic ordering and makes the Fourier couple $Q[S(Q) - 1]$/PDF an experimental quantity well-suited to study the structure of materials with limited structural coherence. That $Ag_{0.4}MoS_2$ is such a material is clearly seen in Figure 2 showing the experimental PDF decaying to zero already at ~22−25 Å. In contrast, the PDF of a perfectly crystalline compound such as 2H−MoS_2 persists to very long real space distances (see Figure 2b in ref 12b).

Results

The atomic PDF technique has been the approach of choice in characterizing glasses and liquids for a long time.[16,18] Its application to crystalline materials with considerable intrinsic disorder coupled with the ability to perform structure determination and even structure refinement is relatively recent.[19,20] The PDF-based structure determination begins with the selection of a plausible structural model including a unit cell and atomic coordinates. A model PDF is calculated and compared with the experimental one. Structural parameters such as unit cell constants, atomic positions, and thermal factors are then refined in a way similar to other structure refinement procedures (e.g., Rietveld analysis) in order to improve the agreement between the calculated and the experimental PDFs. An important difference between Rietveld and PDF analyses is that with the latter the structure determination is directed by the experimental PDF data in real space, whereas with the former it is directed by the diffraction pattern in reciprocal space. The refinement fit was done with the program PDFFIT[21]. In comparing with experiment, the model PDF is convoluted with Sinc function, $S(r) = \sin(Q_{max}r)/r$, to account for the truncation of the experimental data at Q_{max}. The refinement process is terminated when all important details in the experimental PDF are well-reproduced. The usual goodness-of-fit indicator, R_G,

$$R_G = \left\{ \frac{\sum w_i (G_i^{exp} - G_i^{calcd})^2}{\sum w_i (G_i^{exp})^2} \right\}^{1/2} \quad (4)$$

is used to estimate the success of the structure determination and to discriminate between competing structure models. Here, G^{exp} and G^{calcd} are the experimental and calculated PDFs, respectively, and w_i is the weighting factor reflecting the statistical quality of the individual data point. The agreement factor R_G introduced by eq 4 tends to be greater than the agreement factors reported in most single-crystal and Rietveld refinements. This does not indicate an inferior structure refinement but merely reflects the fact that the PDF function being fit is very different from the one fit in a single-crystal or Rietveld refinement. Unlike the latter, which represents a function minimized in reciprocal space, R_G represents a function minimized in real space. By nature, this quantity is much more sensitive to local atomic ordering. As a result, R_G values higher than 20% are common with PDF structure determinations.[12,20] The inherently higher absolute value of the goodness-of-fit factors resulting from PDF-based refinements does not affect its functional purpose as a residuals function that must be minimized to find the best fit and as a quantity allowing to differentiate between competing structural models.

To determine the structure of $Ag_{0.4}MoS_2$, we constructed several models using the reported structures of 2H−MoS_2, $LiMoS_2$, and restacked WS_2 as trial ones. In all models, we adjusted the (MoS_2) interlayer distance according to the position of the first Bragg peak in the experimental XRD data (d_{002} = 6.917 Å) and then positioned the Ag atoms in appropriate interlayer sites with distinct local symmetry (e.g., tetrahedral, octahedral, linear, etc.). The first structural model examined was based on the 2H−MoS_2 structure type (space group $P6_3/mmc$)[22] with silver atoms having two sulfur atoms as nearest neighbors (i.e., linear S−Ag−S units).[23] As can be seen in Figure 2a, the model fails to reproduce the basic features of the experimental PDF, in particular the strong feature at 3.2 Å. Two other models based on 2H−MoS_2 type structure with Ag atoms in tetrahedral and octahedral coordination were considered as well. These models showed even larger disagreement with the experimental PDF data and indicated that the atomic ordering in Ag-intercalated MoS_2 is substantially different from that in pristine MoS_2.

Next, we turned our attention to structure models of lower overall crystallographic symmetry and considered the structure of $LiMoS_2$ as a starting point. One model was constructed by substituting Ag^+ for Li^+ ions in the triclinic structure of $LiMoS_2$ (space group $P\bar{1}$) predicted by ab initio model calculations.[24] The model performed somewhat better but still could not reproduce important details in the experimental PDF data (see Figure 2b). Another model was constructed by substituting Ag^+ for Li^+ ions in another triclinic $LiMoS_2$ structure found by our previous PDF studies (space group $P\bar{1}$).[12b] This model also displayed marked disagreement with the experimental data (see Figure 2c). The results showed that although Ag^+ and Li^+ are of the same valence state in the MoS_2 host, they do not adopt similar local environments.

Finally, we approached the structure of $Ag_{0.4}MoS_2$ by considering the atomic arrangement found in restacked WS_2.[12] Three models were constructed featuring three possible local environments for Ag^+ ions with linear, octahedral, and tetrahedral coordination of sulfur atoms, respectively, according to the constraints of space group $P112_1$. As can be seen in Figure 3, the models with Ag in octahedral (Figure 3c) and tetrahedral coordination (Figure 3b) are capable of reproducing some of the basic features of the experimental PDF data but fail in the details. From all models considered, only the one with almost linear S−Ag−S units reproduces all details in the experimental data (Figure 3a). The corresponding R_G value was 33.8%, which is comparable to the previously reported R_G values for "restacked" WS_2 and $LiMoS_2$. Considering that $Ag_{0.4}MoS_2$ was prepared by a soft chemistry encapsulative restacking route and hence possesses a high degree of disorder, the level of agreement achieved is quite good and acceptable. The refined structural parameters are presented in Table 1. Selected bond distances and bond angles are summarized in Table 2.

Discussion

As the results of the PDF study show, the 3D structure of Ag-intercalated MoS_2 is well-described in a monoclinic unit cell (space group $P112_1$) with cell constants a = 3.250(1) Å, b = 5.706(1) Å, c = 13.867(3) Å, and γ = 89.77°. There are four formula units of $Ag_{0.4}MoS_2$ in the cell. The occupancy of Ag ions on (2a) positions refined to a value of 0.74, leading to the stoichiometry of $Ag_{0.37}MoS_2$, in good agreement with the

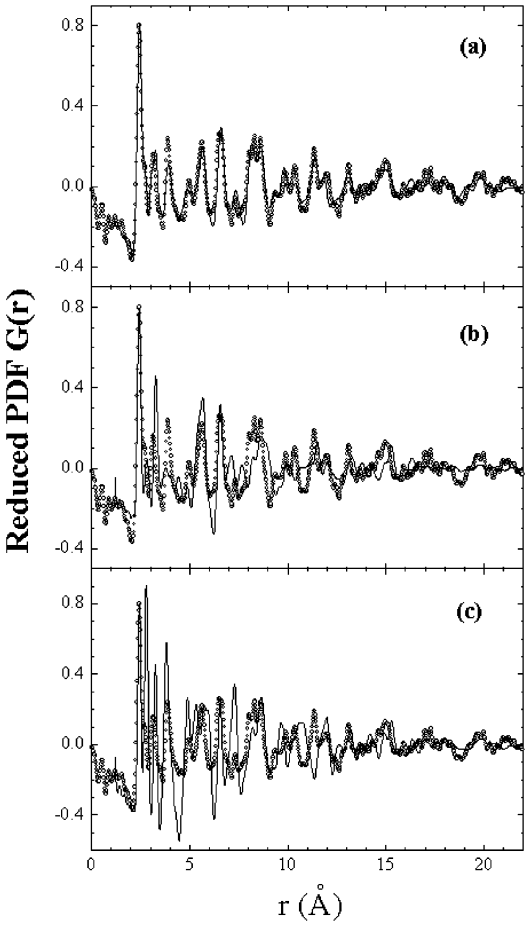

Figure 3. Comparison between the experimental PDF for $Ag_{0.4}MoS_2$ (circles) and model PDFs (line) based on the monoclinically distorted WTe_2 type structure occurring in restacked WS_2. Model (a) features linear AgS_2 units, (b) tetrahedral AgS_4 units, and (c) octahedral AgS_6 units.

TABLE 1: Positional Parameters (*x,y,z*) and Isotropic Thermal Displacement Factors, U_{ij}, of Ag, Mo, and S Atoms in $Ag_{0.4}MoS_2$ as Determined by a PDF-Directed Structure Refinement

	x	*y*	*z*	U_{11} (Å^2)	U_{22} (Å^2)	U_{33} (Å^2)
Ag(1)	0.3199(12)	0.3594(6)	0.2934(2)	0.0323(7)	0.0320(8)	0.0121(6)
Mo(1)	0.9679(3)	0.7307(1)	0.5106(1)	0.0145(1)	0.0075(1)	0.0380(4)
Mo(2)	0.4944(3)	0.8849(1)	0.0464(1)	0.0145(1)	0.0075(1)	0.0380(4)
S(1)	0.0084(13)	0.0086(3)	0.6541(1)	0.0140(3)	0.0100(2)	0.0193(5)
S(2)	0.4654(10)	0.4928(4)	0.1322(1)	0.0140(3)	0.0100(2)	0.0193(5)
S(3)	0.5770(4)	0.1244(5)	0.8948(1)	0.0140(3)	0.0100(2)	0.0193(5)
S(4)	0.0045(14)	0.3333(5)	0.4543(1)	0.0140(3)	0.0100(2)	0.0193(5)

chemical formula $Ag_{0.4}MoS_2$ determined from microprobe EDS analyses. A fragment of the crystal structure is shown in Figure 4.

As shown in Figure 5a, Ag atoms have two nearest S neighbors at 2.41 and 2.46 Å making a bond angle, S−Ag−S, of 160.6°. The presence of only two S atoms around Ag is in agreement with the results of recent EXAFS studies.[8a] The average Ag−S bond distance is consistent with those determined from the EXAFS experiments and crystallographic (Ag−S) bond distance in Ag_2S (2.43 Å).[25]

In addition to the two nearest sulfur neighbors, each Ag ion has three more distant sulfur neighbors at 3.05−3.15 Å (see Figure 5a). These second neighbor atoms are probably responsible for the marked deviation of the S−Ag−S angle from the ideal 180°. If these three second neighbor sulfur atoms are considered to be at a weakly bonding distance, the total coordination environment of Ag becomes highly irregular. Given the large difference in Ag−S distances between the first and the second sulfur atom neighbors, the local structure of the metal is practically linear. The minimum Ag−Ag separation in $Ag_{0.4}MoS_2$ is 3.25 Å and not 2.91 Å as suggested by EXAFS experiments.[8a] Perhaps the 2.91 Å distance can now be explained in terms of the three distant S neighbors at 3.05−3.15 Å.

TABLE 2: Selected Interatomic Distances and Bond Angles in $Ag_{0.4}MoS_2$. The esd's in distances and angles are better than 0.01 Å and 0.1 deg.

atoms	distance (Å)	atoms	angles (deg)
Ag(1)−S(1)	3.05, 3.59	S(1)−Ag(1)−S(2)	160.6
Ag(1)−S(2)	2.41, 3.64	S(1)−Mo(1)−S(2)	77.2, 79.9
Ag(1)−S(3)	3.11, 3.28	S(1)−Mo(1)−S(3)	106.4, 109.3
Ag(1)−S(4)	2.46, 3.15	S(2)−Mo(1)−S(2)	74.7
Mo(1)−Mo(2)	2.70, 2.85	S(2)−Mo(1)−S(3)	99.1, 101.3
Mo(1)−Mo(1)	3.25	S(2)−Mo(1)−S(4)	74.7, 76.6
Mo(2)−Mo(2)	3.25	S(3)−Mo(1)−S(3)	83.8
Mo(1)−S(1)	2.55	S(3)−Mo(1)−S(4)	94.7, 97.7
Mo(1)−S(2)	2.54, 2.80	S(1)−Mo(2)−S(1)	90.4
Mo(1)−S(3)	2.34, 2.53	S(1)−Mo(2)−S(2)	84.2, 87.5
Mo(1)−S(4)	2.40	S(1)−Mo(2)−S(3)	108.9, 118.5
Mo(2)−S(1)	2.28, 2.29	S(1)−Mo(2)−S(4)	90.1, 90.4
Mo(2)−S(2)	2.54	S(2)−Mo(2)−S(4)	76.5, 79.7
Mo(2)−S(3)	2.52	S(3)−Mo(2)−S(4)	76.4, 84.9
Mo(2)−S(4)	2.41	S(4)−Mo(2)−S(4)	84.7

It is interesting to discuss why Ag prefers a 2-coordinate geometry in this case even though it is also capable of adopting higher coordination numbers such as 3, 4, and 6. One reason might be that the trigonal pyramidal sulfur atoms direct their filled p orbitals (lone pair of electrons) perpendicularly to the MoS_2 slabs in the van der Waals space. This makes sulfur somewhat phosphorus-like with a lone pair (mainly a filled p orbital) and available for coordination; see schematic representation in Figure 6. This arrangement is best for linear coordination particularly when atoms with linear bonding propensity such as Cu, Ag, and Au are present in the intralamellar space as we observed.

The MoS_2 slabs in $Ag_{0.4}MoS_2$ are made of severely distorted edge-shared MoS_6 octahedra (Figure 4a,b) just like those found in restacked WS_2. They are very different from those in 2H−MoS_2, which are made of trigonal prismatic MoS_6 units. While there is only one type of first neighbor Mo−S distance of 2.37 Å in 2H−MoS_2, the first neighbor Mo−S distances in $Ag_{0.4}MoS_2$ vary from 2.28 to 2.80 Å, as summarized in Table 2. The distortion of MoS_2 slabs is also documented by the values of S−Mo−S bond angles. In contrast to the unique bond angles of 79.1 and 83.8° in 2H−MoS_2, the S−Mo−S bond angles in $Ag_{0.4}MoS_2$ vary from 74.7 to 118.5°. The severe deformation in MoS_6 coordination sphere reflects the departure of Mo atoms from the positions in their original hexagonal lattice and their shift toward each other to form zigzag chains with Mo−Mo bonds of 2.70 and 2.85 Å; see Figure 5b. The Mo−Mo distances along the *a*- and *b*-axes are estimated to be 3.25 and 3.86−3.95 Å, respectively (see Figure 5b).

The arrangement of Mo atoms in $Ag_{0.4}MoS_2$ is nearly identical to that of W atoms in restacked WS_2.[12a] It is however quite different from the "diamond chain" clustering motif occurring in $LiMoS_2$. This is a consequence of the different oxidation states of Mo atoms in the two compounds. In $Ag_{0.4}MoS_2$, the Mo atoms are formally in a mixed valance state of Mo^{3+} (40%)/Mo^{4+} (60%) whereas in $LiMoS_2$ all Mo atoms are present formally as Mo^{3+} ions. The mixed valence state does not permit a complete interaction with three adjacent Mo ions as in $LiMoS_2$. Instead, it results in only two short Mo−Mo distances.

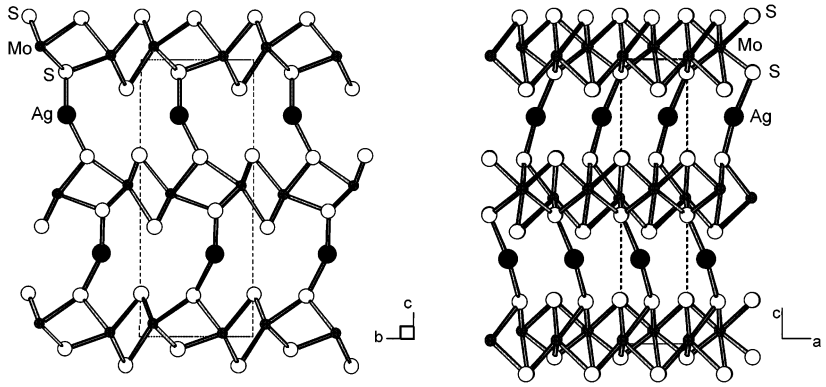

Figure 4. Fragment of the structure of $Ag_{0.4}MoS_2$ as refined by PDFFIT. (a) Viewed down the *a*-axis and (b) viewed down the *b*-axis of the monoclinic unit cell.

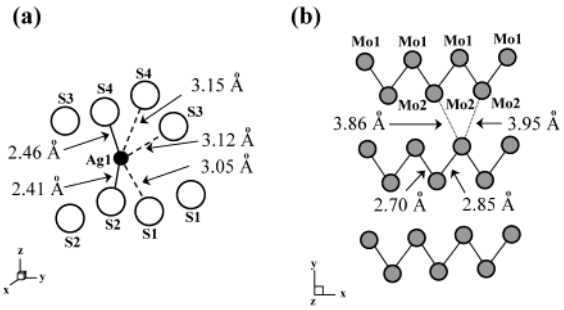

Figure 5. Local atomic arrangement around Ag ions (a) and in Mo−Mo sublattice (b) in $Ag_{0.4}MoS_2$ viewed down the *c*-axis of the monoclinic unit cell. In the figures, the large open, the medium gray-colored, and the small black-colored circles represent S, Mo, and Ag ions, respectively.

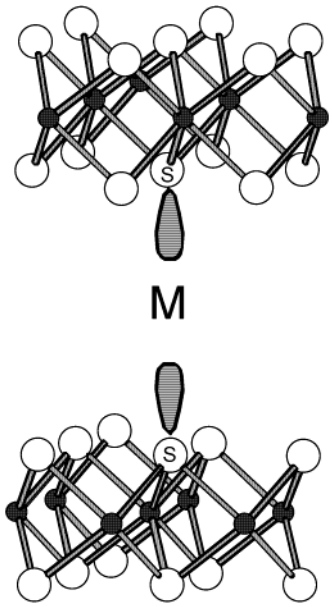

Figure 6. Schematic representation of a structural fragment from MoS_2 showing the direction of the sulfur atom lone pair and its approach toward an intercalated metal atom.

Conclusions

The 3D structure of a MoS_2-intercalated material, Ag_xMoS_2, prepared using soft chemistry, was determined for the first time with the atomic PDF technique. Although disordered over long ranges (>25 Å), Ag_xMoS_2 is a nanocrystalline material with substantial local and intermediate order. At the atomic scale, the structure is a stacked assembly of parallel MoS_2 slabs, made of distorted MoS_6 octahedra and zigzag Mo−Mo chains, sandwiching linearly coordinated Ag atoms. The new structural information obtained for Ag_xMoS_2 could not have been obtained by any other currently available technique. It can be used to better understand and perhaps predict the material's properties and enable sophisticated theoretical calculations to be performed by providing the proper structural model. This work also clearly demonstrates the usefulness and power of the PDF technique in studying the structures of highly disordered, poorly diffracting, and nanocrystalline materials.

Acknowledgment. This work was supported by NSF (CHE 99-03706 and DMR-9817287), DOE (DE-FG02-97ER45651). The Advanced Photon Source is supported by DOE under Contract No. W-31-109-Eng-38.

References and Notes

(1) (a) Joensen, P.; Frindt, R. F.; Morrison, S. R. *Mater. Res. Bull.* **1986**, *21*, 457. (b) Gee, M. A.; Frindt, R. F.; Joensen, P.; Morrison, S. R. *Mater. Res. Bull.* **1986**, *21*, 543. (c) Gordon, R. A.; Yang, D.; Crozier, E. D.; Jiang, D. T.; Frindt, R. F. *Phys. Rev. B (Cond. Matter Mater. Phys.)* **2002**, *65*, 125407/1−9.

(2) (a) Kanatzidis, M. G.; Bissessur, R.; DeGroot, D. C.; Schindler, J. L.; Kannewurf, C. R. *Chem. Mater.* **1993**, *5*, 595. (b) Bissessur, R.; Kanatzidis, M. G.; Schindler, J. L.; Kannewurf, C. R. *J. Chem. Soc., Chem. Commun.* **1993**, 1582. (c) Wang, L.; Schindler, J.; Thomas, J. A.; Kannewurf, C. R.; Kanatzidis, M. G. *Chem. Mater.* **1995**, *7*, 1753. (d) Wang, L.; Kanatzidis, M. G. *Chem. Mater.* **2001**, *13*, 3717.

(3) (a) Miremadi, B. K.; Morrison, S. R. *J. Appl. Phys.* **1988**, *63*, 4970. (b) Frindt, R. F.; Yang, D. *Mol. Cryst. Liq. Cryst.* **1998**, *311*, 775. (c) Oriakhi, C. O.; Nafshun, R. L.; Lerner, M. M. *Mater. Res. Bull.* **1996**, *31*, 1513. (d) Benavente, E.; Santa Ana, M. A.; Mendizábal, F.; González, G. *Coord. Chem. Rev.* **2002**, *224*, 87.

(4) Soft Chemistry Routes to New Materials—Chimie Douce—International Symposium, Materials Science Forum, 1994, Vol. 152−153 and papers therein.

(5) (a) Yang, D.; Westreich, P.; Frindt, R. F. *Nanostruct. Mater.* **1999**, *12*, 467. (b) Yang, D.; Frindt, R. F. *J. Phys. Chem. Solids* **1996**, *57*, 1113. (c) Zhou, X.; Yang, D.; Frindt, R. F. *J. Phys. Chem. Solids* **1996**, *57*, 1137.

(6) Heising, J.; Bonhomme, F.; Kanatzidis, M. G. *J. Solid State Chem.* **1998**, *139*, 22.

(7) (a) Bissessur, R.; Heising, J.; Hirpo, W.; Kanatzidis, M. G. *Chem. Mater.* **1996**, *8*, 318. (b) Brenner, J.; Marshall, C. L.; Ellis, L.; Tomczyk, N.; Heising, J.; Kanatzidis, M. G. *Chem. Mater.* **1998**, *10*, 1244.

(8) (a) Allen, P. G.; Gash, A. E.; Dorhout, P. K.; Strauss, S. H. *Chem. Mater.* **2001**, *13*, 2257. (b) Golub, A. S.; Shumilova, I. B.; Zubavichus, Y. V.; Slovokhotov, Y. L.; Novikov, Y. L.; Marie, A. M.; Danot, M. *Solid State Ionics* **1999**, *122*, 137.

(9) (a) Lemaux, S.; Golub, A. S.; Gressier, P.; Ouvrard, G. *J. Solid State Chem.* **1999**, *147*, 336. (b) Gash, E. A.; Spain, A. L.; Dysleski, L. M.; Flashenriem, C. J.; Kalaveshi, A.; Dorhout, P. K.; Strauss, S. H. *Environ. Sci. Technol.* **1998**, *32*, 1007.

(10) Heising, J.; Kanatzidis, M. G. *J. Am. Chem. Soc.* **1999**, *121*, 11720−11732.

(11) Dungey, K. E.; Curtis, M. D.; Penner-Hahn, J. E. *Chem. Mater.* **1998**, *10*, 2152.

(12) (a) Petkov, V.; Billinge, S. J. L.; Heising, J.; Kanatzidis, M. G. *J. Am. Chem. Soc.* **2000**, *122*, 11571. (b) Petkov, V.; Billinge, S. J. L.; Larson,

P.; Mahanti, S. D.; Vogt, T.; Rangan, K. K.; Kanatzidis, M. G. *Phys. Rev. B* **2002**, *65*, 11571.

(13) Heising, J.; Kanatzidis, M. G. *J. Am. Chem. Soc.* **1999**, *121*, 638.

(14) Rietveld, H. *J. Appl. Crystallogr.* **1968**, *2*, 65.

(15) Tsai, H. L.; Heising, J.; Schindler, J. L.; Kannewurf, C. R.; Kanatzidis, M. G. *Chem. Mater.* **1997**, *9*, 879.

(16) Klug, H. P.; Alexander, L. E. *X-ray Diffraction Procedures for Polycrystalline Materials*; Wiley: New York, 1974.

(17) Petkov, V. *J. Appl. Crystallogr.* **1989**, *22*, 387.

(18) (a) Yin, C. D.; Okuno, M.; Morikawa, H.; Marumo, F. *J. Non-Cryst. Solids* **1983**, *55*, 131. (b) Elliott, S. R.; Rayment, T.; Cummings, S. *J. Phys. Colloq.* **1982**, *43C*, 35. (c) Fowler, T. G.; Elliott, S. R. *J. Non-Cryst. Solids* **1982**, *53*, 43. (d) Konnert, J. H.; D'Antonio, P.; Karle, J. *J. Non-Cryst. Solids* **1982**, *53*, 135.

(19) Billinge, S. J. L.; DiFrancesco, R. G.; Kwei, G. H.; Neumeier, J. J.; Thompson, J. D. *Phys. Rev. Lett.* **1996**, *77*, 715.

(20) (a) Egami, T. *Mater. Trans.* **1990**, *31*, 163. (b) Teslic, S.; Egami, T. *Acta Crystallogr.* **1998**, *B54*, 750. (c) Tucker, M.; Dove, M.; Keen, D. A. *J. Phys. Condens. Mater.* **2000**, *12*, L723.

(21) Proffen, Th.; Billinge, S. J. L. *J. Appl. Crystallogr.* **1999**, *32*, 572.

(22) Bronsema, K. D.; De Boer, J. L.; Jellinek, F. *Z. Anorg. Allg. Chem.* **1986**, *540*, 15.

(23) We have also examined the models of trigonal 1T-MoS_2 structure (space group *P*3 from ref. 11) with Ag ion in appropriate interlayer sites and found them to be equally unsatisfactory.

(24) Rocquefelte, X.; Boucher, F.; Gressier, P.; Ouvrard, G.; Blaha, P.; Schwarz, K. *Phys. Rev. B* **2000**, *62*, 2397.

(25) Cava, R. J.; Reidinger, F.; Wuensch, B. J. *J. Solid State Chem.* **1980**, *31*, 69.